Application of Complex Geophysical Methods for the Detection of Unconsolidated Zones in Flood Dikes

Tomislaw Golębiowski, Bogdan Piwakowski, Michal Ćwiklik

remote sensing

MDPI

Article

Application of Complex Geophysical Methods for the Detection of Unconsolidated Zones in Flood Dikes

Tomisław Gołębiowski [1], Bogdan Piwakowski [2] and Michał Ćwiklik [1,*]

[1] Faculty of Environmental and Power Engineering, Cracow University of Technology, Warszawska St. 24, 31-155 Cracow, Poland; tgolebiowski@pk.edu.pl
[2] Institute d'Electronique, Microelectronique & Nanotechnologies Cité Scientifique, Ecole Centrale de Lille CS 20048, CEDEX, 59-651 Villeneuve d'Ascq, France; bogdan.piwakowski@centralelille.fr
* Correspondence: michal.cwiklik@doktorant.pk.edu.pl

Abstract: The flood levees in the vicinity of Krakow city (Poland) are, in some places, over 100 years old. Thereupon, in the flood dike, and its subsoil, can appear unconsolidated zones, which, during the flood stage, can be a simple way of water flow and/or even can be the place where the levee body will be destroyed. This phenomenon took place in Wawrzeńczyce village, near Krakow city, during the flood in 2010. The geophysical research was carried out, in order to develop a methodology of recognition of potential areas where the levee body can be damaged. The geophysical surveys were conducted with the use of electrical and electromagnetic methods, as well as utilizing the seismic method. The general identification of examined media was realized by the electrical resistivity tomography (ERT) method. The ERT surveys were supplemented by capacitively-coupled resistivity (CCR) measurements, in order to analyze the usefulness of the CCR method for the examination of river dikes and reduction of interpretation ambiguity. The ground penetrating radar (GPR) method detected small anomalies in the body dike, due to the very high resolution of this method, which were not detected by the ERT and CCR techniques. During GPR surveys, non-standard measurement techniques were applied. Finally, the high-resolution seismic reflection (HRSR) method provided a clear and high-resolution image of the dike structure up to the water table and assisted with the identification of the hazard non-consolidated zones.

Keywords: disaster relief; recoveryand reconstruction; environmental engineering; geoelectrical and electromagnetics methods; high-resolution seismic

Citation: Gołębiowski, T.; Piwakowski, B.; Ćwiklik, M. Application of Complex Geophysical Methods for the Detection of Unconsolidated Zones in Flood Dikes. *Remote Sens.* **2022**, *14*, 538. https://doi.org/10.3390/rs14030538

Academic Editors: Hideomi Gokon, Yudai Honma and Shunichi Koshimura

Received: 8 December 2021
Accepted: 13 January 2022
Published: 23 January 2022

1. Introduction

Fluvial levees are crucial hydrotechnical constructions for protecting human lives and activities. Regrettably, the technical condition of levees in many countries is not satisfactory, for example, visible landslides, seepage, etc. As an example, statistics from Poland show that over 60% of the whole levee is over 50 years old. Furthermore, there are still some places where the operated levees are over 100 years old [1]. An identical situation was in Wawrzeńczyce village, near Krakow city (Poland), where during the flood in 2010, the part levee was completely destroyed after this the levee was rebuilt. However, there are plenty of places where a similar situation can appear. Thereupon, in our research, we try to develop a methodology to be able to find potential places where during the next flood stage the levee body can be destroyed and/or the first symptoms, such as leakages, may be spotted. Therefore, in the first step we perform literature study, in order to find the best, non-invasive geophysical method.

In general, there are many geophysical methods that may be applied for the examination of a flood dike and its subsoil; mostly electrical and electromagnetic methods were applied for this purpose, i.e., the standard (i.e., short-offset reflection profiling) ground penetrating radar (GPR) method, which is typically used as a profiling method [2–4], or

non-standard GPR surveys [5–13], in which the different antenna orientations can be used to provide a more reliable picture of the internal structure of the levee or can to provide the GPR attributes to pick weak zones in the levees. One of the most used methods, in this case, is also electrical resistivity tomography (ERT), also called the resistivity imaging (RI). In most cases, the 2D ERT technique was applied [14–23]. It is worth mentioning that the aforementioned methods are the common applied techniques and most effective for studying the internal structure of levees. The electromagnetic profiling (EMP) method, also called the ground conductivity meter (GCM), is less popular than the previous one and It uses relatively fast recognition of the levee [15–26]. Amongst seismic methods, the refraction and multichannel analysis of surface waves (MASW) techniques are applied for this purpose [27,28]. As far as we know, there are no recommendations on the use of the high-resolution seismic reflection (HRSR) [29,30] for the inspection of dikes, but this technique seems to be a useful geophysical method for the detection of small unconsolidated zones, due to its high resolution [31–33]. Occasionally, other geophysical methods are used, e.g., the microgravimetric technique [34], fast growing capacitively coupled resistivity (CCR) [35–38] method, very low frequency (VLF) method, radio-magnetotelluric (MT) method, infrared (IR) method, self-potentials (SP) method, and LiDAR technique [39,40].

Based on the performed analysis, for our study, we choose the GPR, ERT, and seismic methods. We also planned to test capacitively coupled resistivity method (CCR), which, in the literature, is considered as the method gaining popularity. We also spotted that the problem is the introduced methods are very often used separately. That provides an additional ambiguity to the results of the geophysical research. To avoid this, a comprehensive geophysical approach should be used, involving a few geophysical methods that complement each other, and the geotechnical methods that should also help to answer if there any clear geological/geotechnical symptoms that can cause a geophysical anomaly.

2. Study Area

Terrain surveys were carried out in southern Poland (Figure 1A), on the Vistula river flood dike in the village of Wawrzeńczyce, near Cracow (Figure 1B). Detection and monitoring of development of unconsolidated zones, in which water paths occur, is crucial because such zones may lead to leakages (Figure 1C) or even the damage of flood dikes and other hydrotechnical infrastructures (Figure 1D) during flooding. Such a situation was observed in the investigation site, during the flood of 2010 (Figure 1C,D).

Geophysical, geological, and geotechnical investigations were performed on the flood dike in the area surrounding flood gate. no. 1 (Figure 1C); the dike in the investigation site was built before World War II and renovated in the years 1970–1972. During the flood of 2010, the water channel and concrete flood gate no. 1 were destroyed (Figure 1D); in the body of the dike, the leakages were observed (Figure 1C). After the flood, the water channel, flood gate, and dike in place no. III were reconstructed (Figure 1E). Other parts of the dike, where leakages were observed during the flood, were only protected with bags filled with sand (Figure 1C), and no renovation was carried out.

The geophysical surveys on the flood dike in the region of flood gate no. 1 were conducted in years 2014–2019, in two main stages, i.e.:

- Stage I (with few substages)—between 2014–2018—preliminary geophysical surveys, with the application of the GPR, ERT, and EMP methods, as well as DPL (dynamic penetration light) soundings and geological drillings, were carried out, mainly north of flood gate no. 1 (Figure 1C—over leakages no. III, IV, and V); the selected results, obtained at this stage, were presented in various scientific conferences [6,9].
- Stage II—2019—detailed geophysical surveys, with application of the GPR, ERT, CCR, and seismic methods, as well as DPL soundings and geological drillings, were performed, mainly south of flood gate no. 1 (Figure 1C—over leakages no. I and II); the results of numerical modelling, carried out for the GPR and ERT methods, were presented at a scientific conference [9].

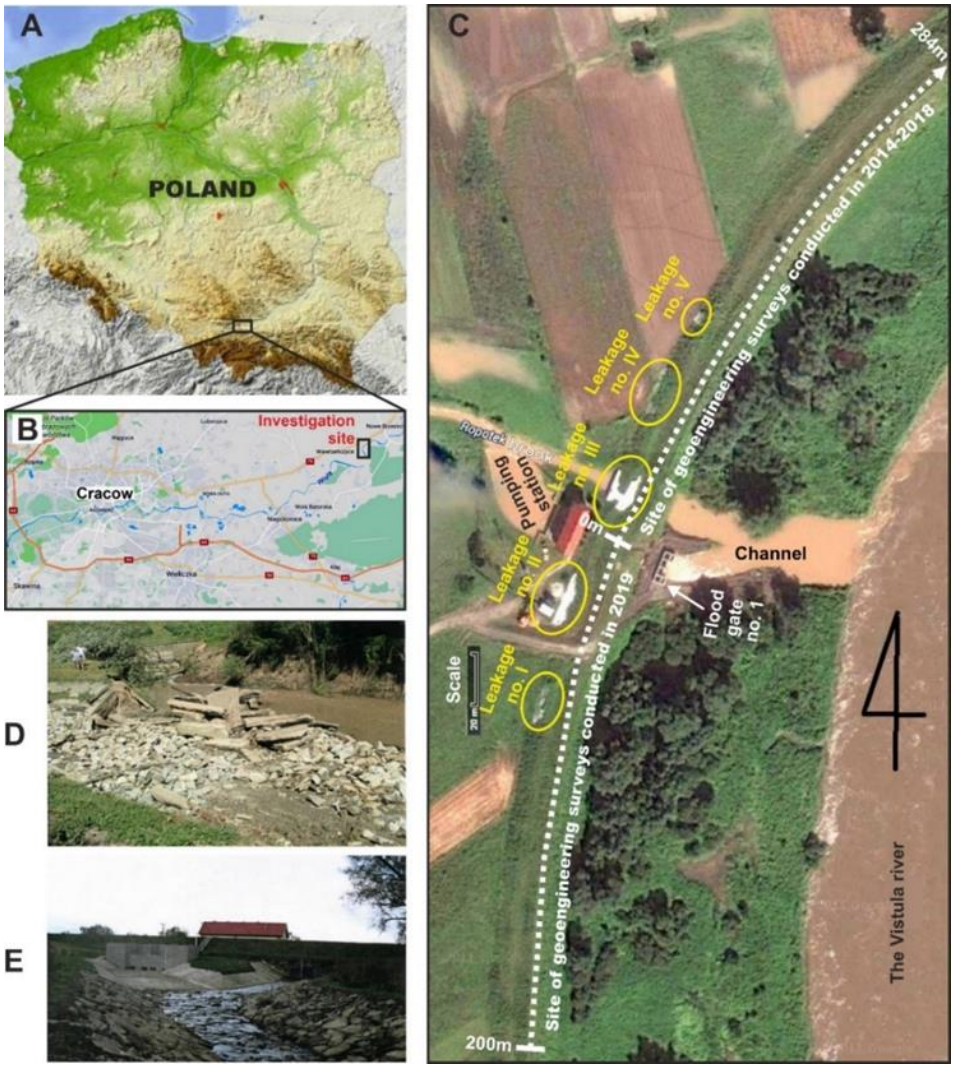

Figure 1. (**A**) General location of the investigation site; (**B**) Detailed location of the investigation site on the Vistula river dike near in the village of Wawrzeńczyce near Cracow (map: www.google.pl/maps), access date: 1 January 2022; (**C**) Flood gate no. 1 during the flood in 2010 and the surrounding area [41]; (**D**) Flood gate and water channel after the flood in 2010 [41]; (**E**) Flood gate and water channel after renovation [41].

The results of the preliminary investigations (between 2014–2018) delivered general information about the distribution of geophysical anomalies in the examined dike and its subsoil. However, the detailed and unequivocal identification of where anomalies should be correlated with unconsolidated zones was difficult, and this was compounded by the different materials used in the construction of the dike. Therefore, in the second stage of geophysical surveys, additional CCR, and seismic methods were applied, and complex geophysical–geological–geotechnical interpretation was carried out to detect, with high probability, the location of unconsolidated zones, i.e., zones with higher water permeability, in the dike and its subsoil.

In this paper, the results obtained during the surveys, carried out in 2019 in the southern part of the dike (Figure 1C), are presented (currently, we do not have a formal consent to provide geophysical measurements). Besides the application of the GPR, ERT, and CCR methods, the novel technique, the HRSR method, which was not used in previous investigations, was introduced. Figure 2A presents the location of the GPR, ERT, CCR, and HRSR profiles and points of geological drilling and geotechnical soundings.

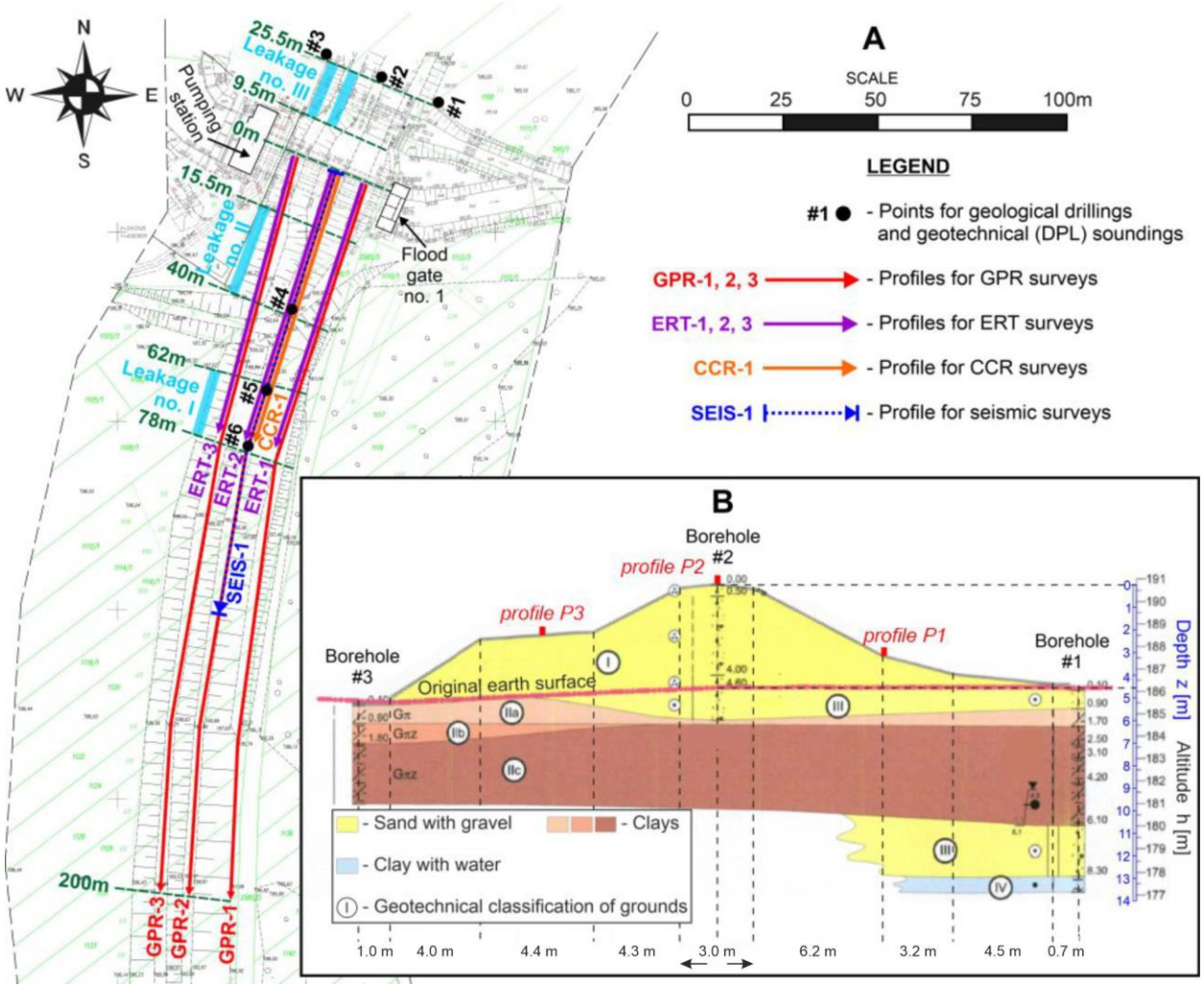

Figure 2. (**A**) Location of GPR, ERT, CCR, and HRSR profiles, as well as points for geological drillings and geotechnical soundings; (**B**) typical cross-section of the examined dike [41].

Before starting the geophysical surveys, geodetic measurements were made (Figure 2A), which delivered the following information: (a) the altitude of the crown of the dike varies from 190.8 m to 191.1 m a.s.l., and the average values are equal to 190.9 m a.s.l.; (b) the altitude of the shelf on the air-side of the dike varies from 188.3 m to 189.3 m a.s.l., and the average values are equal to 188.7 m a.s.l.; (c) the altitude of the shelf on the water-side of the dike varies from 186.7 m to 188.5 m a.s.l., and the average values are equal to 187.6 m a.s.l. The average height of the examined dike is equal to 4.5 m (Figure 2B). Due to the small denivelations, the mean values of altitudes with flat surfaces were assumed in further analyses.

The next stage was to perform geological drillings and DPL soundings, which were carried out on the six positions indicated in Figure 2A; these works were performed in places where leakages were observed during the last flood, in 2010.

As shown in Figure 2B, the body of dike is built mainly of a mixture of sand and gravel (layer no. I). Geological information from the investigation site shows that the subsoil of the examined flood dike is built mainly of Miocene clays (Figure 2B—layers no. IIa, IIb, IIc and IV). Clays are covered by fluvio-glacial and fluvial sand and gravel (Figure 2B—layer no. III). Laboratory tests, carried out on the ground samples taken from the boreholes, revealed that clays no. IIa, IIb, and IIc create an impermeable layer, due to their extremely low water permeability, and leakages should be observed, rather, in the fluvio-glacial and

fluvial sand and gravel (layer no. III), as well as in unconsolidated zones in the body of dike (layer no. I).

During the drillings, the first underground water table was observed at the boundary between layers no. IIc and III, at an altitude of c.a. 180.0 m a.s.l. (Figure 2B). Taking into account the geodetical information presented above, it may be assumed that the first water table should be recorded in geophysical data at a depth of c.a. 11 m, when counting from the crown of a dike; it is obvious that this value may vary, depending on the degree of thickness of layers IIa, IIb, and IIc, as well as the thickness of the shallowest aquifer (layer no. III) along geophysical profiles.

In the body of the examined dike, geotechnical DPL soundings were performed (Figure 3), which indicated that the body of dike is composed mostly of semi-compacted material (where the number of hits was between 5 and 20); in several sub-areas, loose zones (where the number of hits was below 5) and compacted material (where the number of hits was greater than 20) were present in the examined dike. In Figure 3, the positions of leakage zones no. I and II were moved from the air-side of the dike to the vertical plane, cutting the crown of the examined dike; therefore, one should not simply correlate the locations of the leakages with zones of different compactions; it is very probably that the inner water path in the body of the dike, in the region of leakage II, is located in the central part of the dike, between a depth of 0.5–3.0 m, while in the land-site, this path occurs at a depth of c.a. 3.5–4.0 m. The above information suggests that leakage zones are probably correlated with unconsolidated and semi-compacted material. This same situation is observed in the region of leakage no. I.

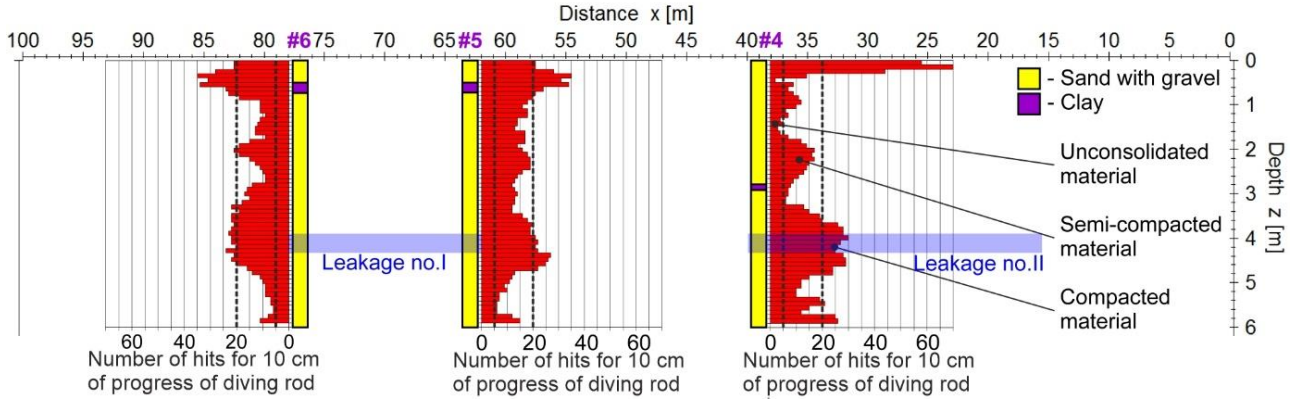

Figure 3. Information from geological boreholes and DPL soundings.

After gathering all the necessary data (i.e., geodetical, geological, and geotechnical), geophysical surveys were carried out on the crown and both shelves of the examined dike, along the profiles shown in Figure 2A.

3. Results of Geophysical Investigations

3.1. GPR Surveys

3.1.1. WARR Measurments

The short-offset reflection surveys were preceded by the WARR (wide angle reflection refraction) measurements, which allowed for the determination of a mean velocity of electromagnetic (em) wave [42]; these measurements were carried out along the first 160 m of profile GPR-2 and first 90 m of profile GPR-3 (Figure 2A). The WARR measurements were carried out with the use of a ProEx georadar system (produced by the company MALA, Sweden, Mala—www.guidelinegeo.com, access date: 1 January 2022), along with 200 MHz unshielded antennae; a standard (i.e., co-pole) orientation of the antennae was assumed; to improve the signal/noise ratio, 16-times stacking was applied, and traces were recorded with a constant distance interval $\Delta x = 0.05$ m.

On the crown of the dike, eight WARR surveys were performed (Figure 4A), but only four of them delivered satisfactory results (Figure 4B–E). On the land-side of the dike, 18 WARR surveys were carried out (Figure 5A), but only 4 of them delivered satisfactory results (Figure 5B–E). Where hodographs could not be used (Figures 4 and 5), only direct air wave (DAW) and part of the direct ground wave (DGW) were recorded, which did not permit the proper determination of the velocity of the em wave. The velocity of the DGW varied from 0.066 to 0.088 m/ns, and the velocity of reflected wave (RW) varied from 0.055 to 0.083 m/ns. Reflections recorded in hodographs at t0 = 20 to 30 ns came from GPR anomalies identified in the radargrams (Figure 6), at depths of 1.0–1.5 m; these anomalies will be analysed in the next section.

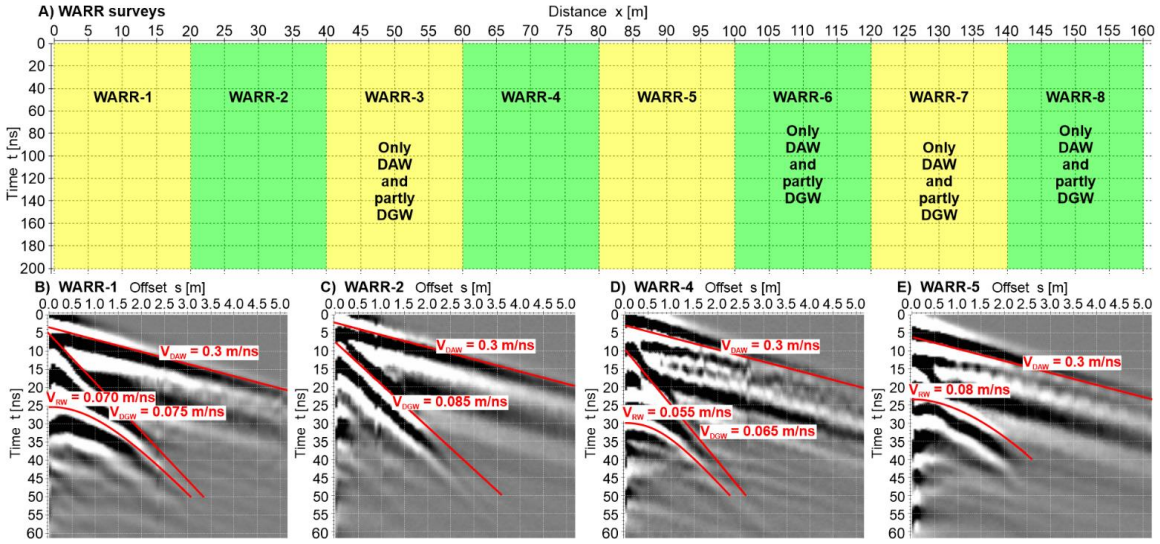

Figure 4. (**A**) Location of WARR surveys along profile GPR-2 (crown of dike); (**B**) First five meters of WARR Hodograph recorded from x = 0 m to x = 20 m; (**C**) First five meters of WARR Hodograph recorded from x = 20 m to x = 40 m; (**D**) First five meters of WARR Hodograph recorded from x = 60 m to x = 80 m; (**E**) First five meters of WARR Hodograph recorded from x = 80 m to x = 100 m.

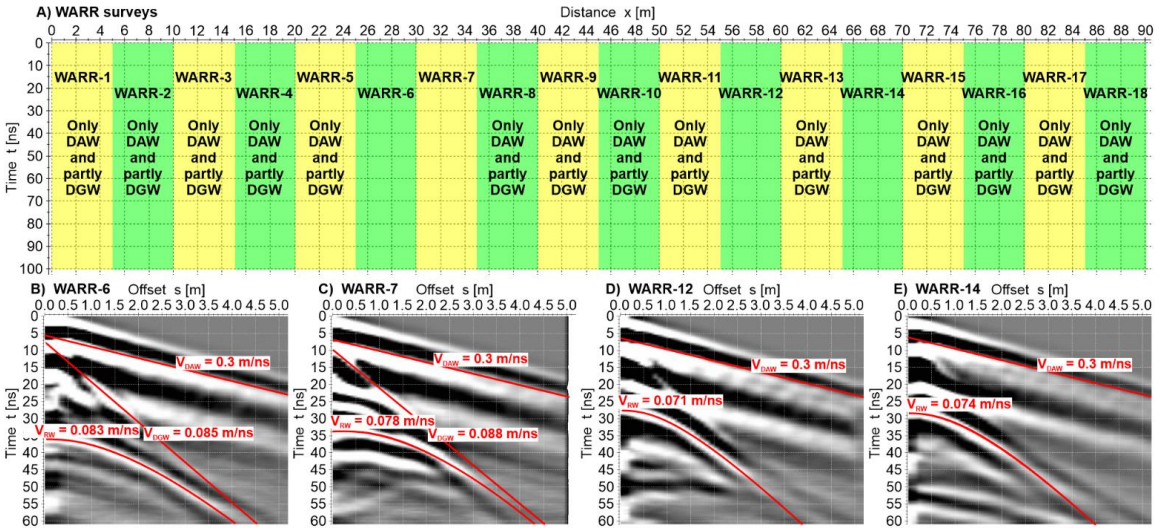

Figure 5. (**A**) Location of WARR surveys along profile GPR-3 (land-side of dike).; (**B**) WARR Hodograph recorded from x = 25 m to x = 30 m; (**C**) WARR Hodograph recorded from x = 30 m to x = 35 m; (**D**) WARR Hodograph recorded from x = 55 m to x = 60 m; (**E**) WARR Hodograph recorded from x = 65 m to x = 70 m.

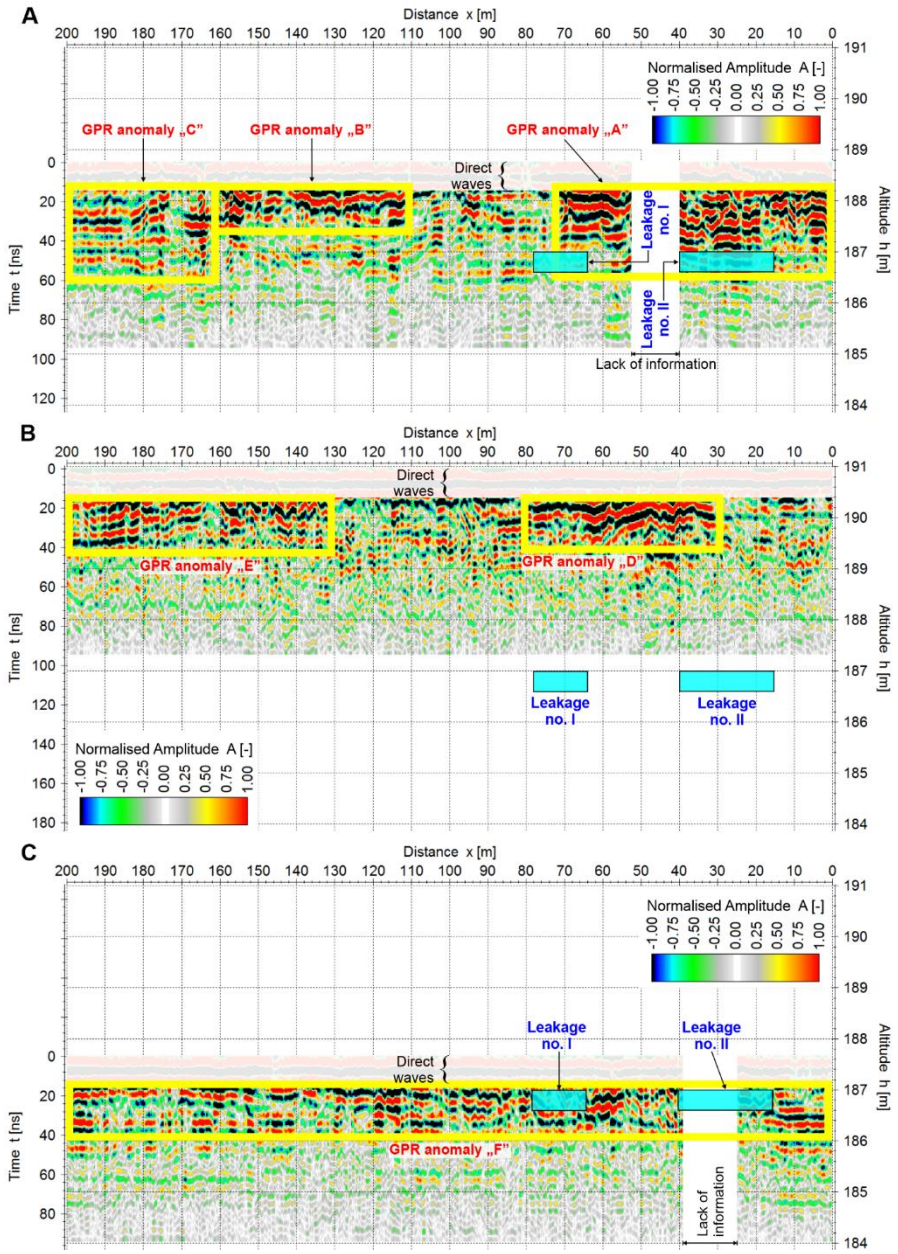

Figure 6. Radargrams recorded along profiles: (**A**) GPR-3—land-side of dike; (**B**) GPR-1—crown of dike; and (**C**) GPR-1—river-site of dike.

Finally, for time-depth conversion of radargrams, a constant mean velocity of em wave equal to 0.077 m/ns was assumed. Typically, velocity for dry sand and gravel varies from 0.1 m/ns to 0.15 m/ns, and results obtained from WARR measurements would indicate that the examined mixture of sand and gravel is wet.

In the next step, detailed GPR reflection surveys were carried out (Figure 6) along three 200-meter profiles (Figure 2A), with the use of a VIY georadar system (produced by Transient Technologies, Ukraine, Kyiv—www.viy.ua, access date: 1 January 2022). A standard (i.e., co-pole) orientation of the antennae, with a frequency of 125 MHz, was applied. The decision to use the VIY georadar set, up with a lower frequency antenna, was reached as a result of unreadable hodographs (Figures 4A and 5A), derived from WARR measurements and the low depth penetration of 200 MHz antennae previously used (Figure 4B–E and Figure 5B–E). Traces were recorded with a constant distance interval of $\Delta x = 0.1$ m. To improve the signal/noise ratio, eight-times stacking was applied during

the data acquisition. All radargrams presented in this paper were subjected to standard signal processing, using the ReflexW software ver.9.5 (www.sandmeier-geo.de, access date: 1 January 2022); a detailed description of radargram processing may be found in the literature [42,43].

3.1.2. GPR Reflection Surveys with Standard Co-Pole Antennae Orientation

Is well-known that attenuation of em waves is a function of conductivity σ for an examined medium. For dry sand and gravel (body of dike—Figure 2B), it may be assumed that typical values of σ should be equal 0.01–0.1 mS/m, which equates to low attenuation. For dry clay (subsoil of dike—Figure 2B) σ = 1.0 mS/m and a higher attenuation is observed in such medium. The presence of water in geological medium causes an increase in conductivity and attenuation, especially in wet clay [42–44]. From the boreholes (Figure 2A), ground samples were taken, and the results of the laboratory tests carried out on these samples revealed that the average value of conductivity for a mixture of sand and gravel was equal to 0.9 mS/m. In such a situation, the conductivity in the body of dike (i.e., in layers no. I and III—Figure 2B) and subsoil (i.e., in layers no. IIa, IIb, and IIc—Figure 2B) is relatively high; therefore, higher attenuation may be expected. Both moisture in the examined medium and local interbeddings of clay in the mixture of sand and gravel (Figure 3) caused a serious reduction of depth range of the 125 MHz antennae; therefore, in Figure 6, readable reflections are visible to depths of 1.5–2 m, whilst the maximum depth penetration of this antennae is c.a. 15 m.

In all radargrams (Figure 6), anomalies were interpreted as follows: (a) high-amplitude anomalies (red and black colours)—unconsolidated material, (b) anomalies with mean amplitudes (navy blue/blue and orange/yellow colors)—semi-compacted material, and (c) low-amplitude anomalies (grey colour)—compacted material. Lack of information in Figure 6A,B (white rectangular) was caused by interferences occurring on the road crossing the dike.

In Figure 6A, the anomaly "A" is observed over leakages no. I and II; in this zone, inner water paths were created during the flood of 2010 and, consequently, the land-side of the dike had to be protected with bags with sand (Figure 1C). Unconsolidated and weathered also material occurs in the region of anomaly "B". In anomaly "C", mainly semi-compacted mixtures of sand and gravel may be distinguished. It is highly probable that, during the next flood, several leakages may appear in the dike, particularly in the strip between altitudes 186.5 and 188.5 m a.s.l.

In Figure 6B, anomaly "D" has similarities with the above anomaly "A" and, equally, a correlation of anomalies "E", "B", and "C" is easily noticed. All mentioned GPR anomalies were caused by the presence of unconsolidated and weathered material in the body of the dike. The top part of the dike, between 188.5–191 m a.s.l., is threatened by the leakages.

In Figure 6C, the GPR anomaly "F" spreads along the whole profile, to depths of 1.5 m; in this strip, a rather semi-compacted mixture of sand and gravel occurs in the dike. Higher amplitudes of reflections in the region of leakages no. I and II illustrate the presence of inner water paths within the body of dike. A reduction of amplitudes in other parts of the anomalous zone "F" was caused by the culmination of sand and gravel by clay material carried by the river during higher water levels. It is highly probable that, during the next flood, several leakages may appear in the dike, particularly in the strip located between altitudes 186–187.5 m a.s.l.

3.1.3. GPR Reflection Surveys with Different Antennae Orientations

The results of the GPR survey carried out on the crown of the dike, with a standard (i.e., co-pole) orientation of the antennae, produced results to a maximum depth of c.a. 2 m (Figure 6B), and it was impossible to record anomalies around leakages no. I and II. Therefore, additional test measurements, with different antennae orientations (shown in Figure 7), were carried out. It should be noted that the majority of georadar systems that are presently available on the market (from amongst other VIY georadars) only allow surveys

to be performed with a standard orientation of the antennae (Figure 7A—option A1), which corresponds to one polarisation of em wave. This paper does not deal with the theoretical description of the propagation of em waves with different polarizations in geological media; further, information on this matter can be found in the geophysical literature [9].

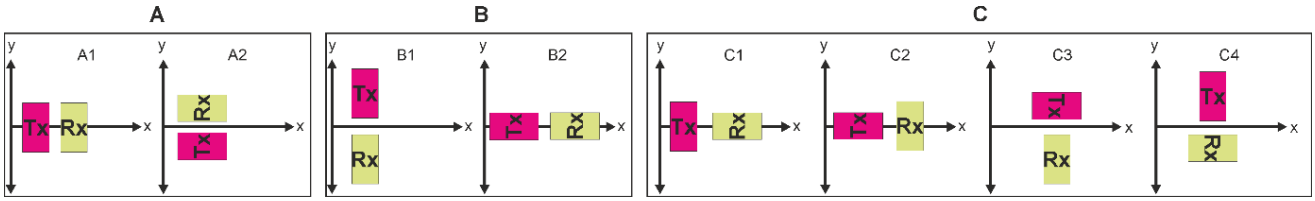

Figure 7. Different orientations of GPR antennae: (**A**) "co-pole" orientations; (**B**) "end-fire" orientations; and (**C**) "cross-pole" orientations.

Test surveys with different antennae orientations (Figure 8) were performed, with the same acquisition parameters and georadar system (i.e., ProEx georadar and 200 MHz antennae), as per the WARR surveys. This system was chosen because it allows us to separate and rotate the Tx and Rx antennae.

Figure 8 shows the results obtained for three different types of orientations. The results recorded for other orientations were omitted because they delivered similar anomaly distributions, i.e., orientations A1 and A2 (Figure 7), B1 and B2, and C1–C3 and C2–C4 delivered similar results.

The standard (i.e., co-pole) orientation (Figure 8A) only permitted the recording of anomalies in the near-surface zone, similar to the surveys carried out with the use of the VIY georadar system (Figure 6B). Therefore, the conclusion may be drawn that the lack of anomalies in the greater depths was not caused by the application of a specific georadar system (i.e., ProEx or VIY) and antennae (i.e., 200 MHz or 125 MHz), but it was an effect of the attenuation of the examined medium and application of a standard orientation antennae (i.e., co-pole) for GPR surveys.

The cross-pole orientations (Figure 8B,C) allowed for the recording of additional high-amplitudes anomalies over leakages no. I and II, and they were caused by the presence of unconsolidated zones, in which the inner water paths were created during the flood of 2010.

The end-fire orientation (Figure 8D) allowed for the detection of new anomalous zones with higher amplitudes, especially between x = 25 m and x = 65 m, as well as from x = 135 m to x = 145 m.

Finally, a novel way of GPR data visualization was proposed based on the special gathering of information from all antennae orientations. Because the radargrams are, in fact, on the matrices with the same horizontal and vertical dimensions (i.e., the same number of traces, distance between traces, number of samples, and time-steps between samples), we have combined in computer program all radargrams (i.e., all matrices) into one 3D matrix, called X. In the next step, the program computed the average amplitude for every sample xij in matrix X, on the basis of the amplitudes of the samples called: aij (from co-pole radargram—Figure 8A), bij (from the cross-pole radargram—Figure 8B), cij (from the cross-pole radargram—Figure 8C), and dij (from the end-fire radargram—Figure 8D). The result of such operations, compared with information from the DPL soundings, is shown in Figure 9. It is clear that combining information from different orientations of antennae into one radargram delivers much better results and enables a more detailed interpretation.

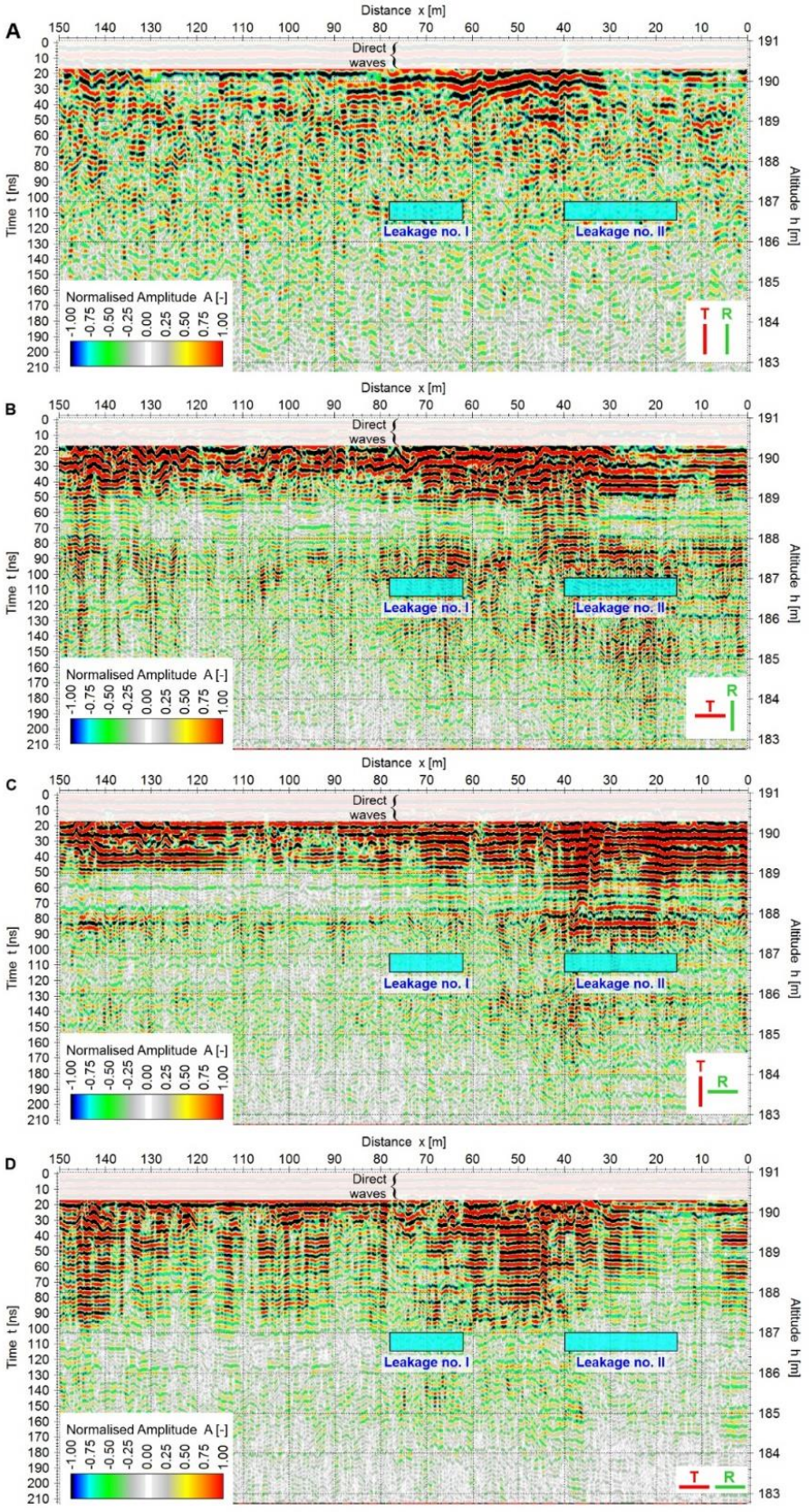

Figure 8. The result of GPR measurements along the crown of a dike with different antennae orientations: (**A**) co-pole, (**B**,**C**) cross-pole, and (**D**) end-fire.

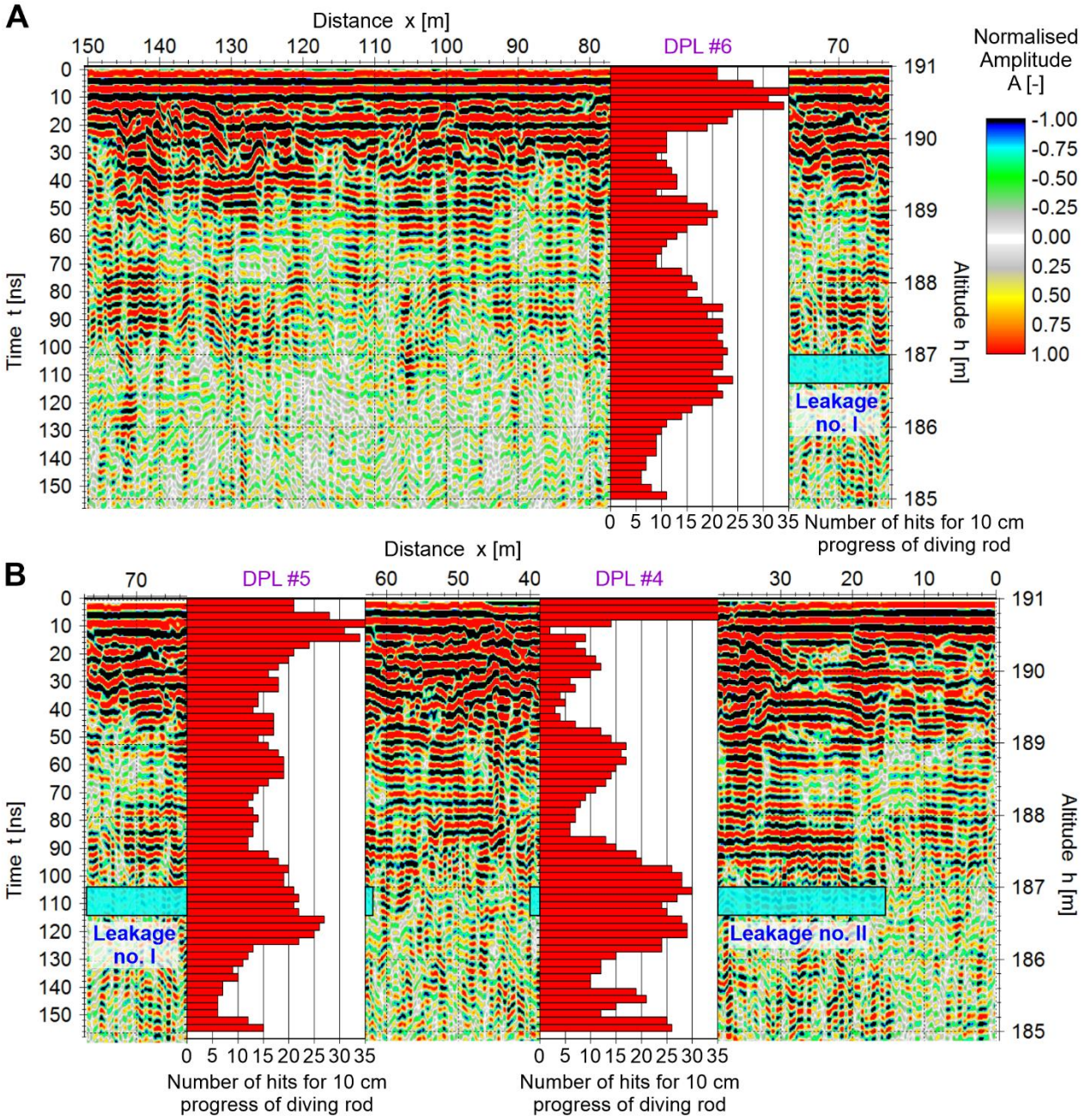

Figure 9. Superposition of information from Figure 8 for different antennae orientations: (**A**) profile section 70 ÷ 150 m; and (**B**) profile section 0 ÷ 70 m.

In Figure 9A, high-amplitudes anomalies, depicting seriously loose and weathered material in the dike, are easily noticed at a depth of c.a. 2 m, i.e., to the altitude c.a. 189 m a.s.l.; it should be stressed here that, in the strip between h = 191 m and h = 190.5 m a.s.l., interpretation is impossible, due to the recording of direct waves, i.e., DAW and DGW. In the strip between altitudes 189 m and 187 m a.s.l., semi-compacted material (i.e., a number of hits between 5–20) occurs in the body of dike, which correlates well with the information from DPL sounding #6. At altitudes from h = 187 m and h = 185 m a.s.l., it is difficult to properly interpret the radargram, due to the high attenuation of the examined medium. Nevertheless, slightly higher amplitudes of reflections were recorded in region where loose and semi-compacted material occurred, i.e., between x = 65 and x = 75 m, from h = 186.5 to h = 185 m.

In Figure 9B, much higher amplitudes were recorded, in comparison to Figure 9A. Similarly, like in Figure 9A, in the strip between h = 191 and h = 190.5 m a.s.l., data interpretation is impossible, due to the recording of direct waves. All anomalies can be observed over leakage no. I and II, and these anomalies may be interpreted as a semi-compacted mixture of sand and gravel, in which the inner water paths were created during the flood of 2010. Seriously unconsolidated zones may be distinguished in subzones of the examined dike, from h = 190.5 to altitudes of 186.5–187 m a.s.l. (number of hits below 5). Taking into account that the average height of the examined dike is c.a. 4.5 m (Figure 2B), the whole body of dike in this area is in a very poor technical condition, which may threaten the stability of the dike during the next flood. The results of DPL soundings #5 and #6 confirm the above geophysical interpretation, i.e., to the depth of 4–4.5 m, mostly semi-compacted material (i.e., a number of hits between 5–20) was noted in this part of the examined dike.

3.2. ERT Surveys

The ERT survey was carried out along the profiles lines 1 to 3 (Figure 2). The total length of each profile is equal 75 m. The survey covers a whole area, which is referred as leakage zone no. 2, and only part of the area is referred to as leakage zone no. 1.

The ERT surveys were made with the basic electrode spacing Δx = 2 m, where lengths of current and potential dipoles a = 1, 2, 5, 9 Δx, and separation factor n, which is ratio of the distance between the current and potential dipole, is equal n = 1, 2, 3, 4, 5. The foregoing parameters resulted in a proper depth and resolution for the necessary investigations [45–47]. The dipole-dipole array was used to obtain the best horizontal resolution [47,48]. The ERT survey was carried out using an Ares II resistivity meter (made by GfInstruments.

The field data was inverted using Res2dinv software [47–49]. A robust inversion [48–51] was applied to the field data. The inversion results are shown in leakage zone no. I–II, and the CCR cross-section (which is discussed in Section 3.3) was also superimposed.

In the resistivity cross-sections, two relatively low anomalies ("L1" and "L2") and one high resistivity anomaly "H" were distinguished.

In Figure 10A, the resistivity anomaly "L1" was observed throughout the whole length of the survey line. Between positions x= 0–25 m of the profile line, the anomaly thickness increased approximately two times. The "L1" anomaly is characterised by a resistivity value of around 250 Ωm. Based on the available geological information (Figure 2B), the aforementioned anomaly consists of sand and gravel—layer no. I. The relatively low resistivity value, versus theoretical values [52], suggests that the previously mentioned sediments are partly mixed with clay.

The low resistivity anomaly "L2" can be observed from 8 m below the ground surface level to the interpreted model boundary. The anomaly is characterized by a resistivity of about 25 Ωm, which clearly indicates the water table presence. Between the "L1" and "L2" anomalies, the high resistivity anomaly "B", with a maximum resistivity value of about 2500 Ωm, was identified. It is worth noting that the general geological cross-section suggests the presence of clays (II a–c) for this depth range. However, the obtained resistivity value is two orders of magnitude too large for this particular lithology [52,53]. The issue explains the data obtained from the holes no. 4 and 5, which shows the sands and gravels present. The relatively high resistivity value of the sand layer suggests that the layer is dry.

In the Figure 10D (waterside), the sand layer from 10–35 m of the survey line is also similar to the landside case. Some changes appear from 35–75 m of the line, where the thickness is increasing. The water table, similar to the previous case, is about 8 m below the ground surface. Bigger differences are visible for the shallowest layer. Its thickness is about 2 times larger than that of the landside case. This can be explained as a result of the Vistula river sediments, which, over time, gradually increased the thickness. Consequently, it caused sands to be mixed with the low resistivity sediments - lay, which was to be expected in this area.

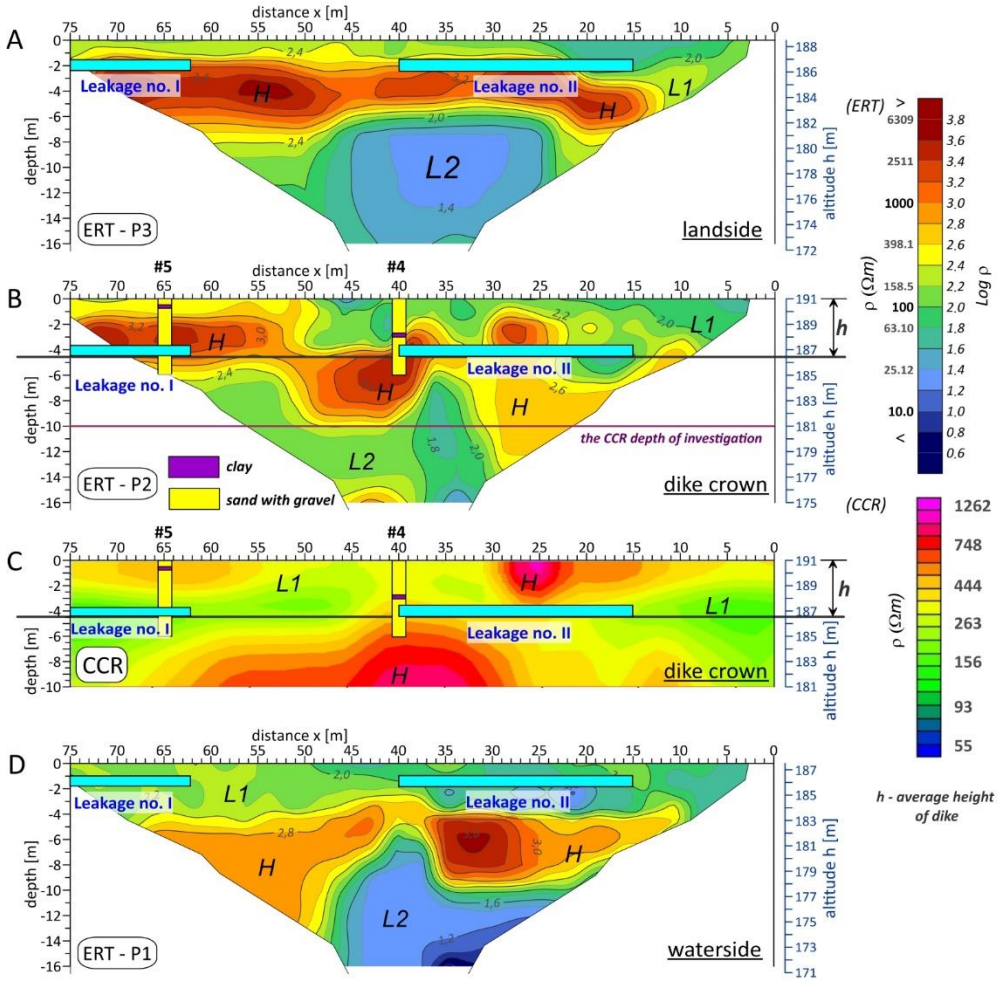

Figure 10. Inverted resistivity cross-sections: (**A**) profile 3, (**B**,**C**) profiles 2 (**D**) profile 1.

The ERT results, obtained from the flood embankment crown, show the presence of sands from 50–75 m of the survey line. The bottom boundary of the aforementioned sediment is correlated with the boundary between the ground and the bank body. The further part of the dike crown is dominated by sand and gravel mixed with clay (Figure 10B), with one exception, between distance x = 22–40, where, again, sand and gravel are noticeable. Below the dike crown, the sediments continue and are visible for the distances x = 8–30 and x = 37–50 m of the profile line.

Additionally, the water table resistivity value is higher than that of the profile P1 and P3, which is connected with the limitation of the inversion technique, where, with increasing depth, the inverted resistivity value is more misfit with the actual resistivity value.

In the matter of selecting the risk zones, it can be said the leakage zones appeared in the dike crown in the places where the dry sands and gravel are present. In addition, the laboratory test results should be taken in account, which prove the sediments are characterised by the extremely high value of water permeability. Thereupon, during the flood stage, where the water table level is increasing, the dry layer of sand and gravel is an excellent medium for water to flow under the dike body. This is possible, assuming that the sand and gravel layer is not present with the layer of sands mixed with clay. An addition of clay prevents further water flow.

In the present case, the biggest problem is that the very same, extremely high permeability sand and gravel sediments constitute building material in some fragments of the dike body. During the flood stage, water flows into the body dike, and the leaks zones appear. It is highly probable that this scenario will be repeated in the future. To sum up,

the ERT methods, with additional geological and laboratory data, afford an explanation of the mechanism of leakage formation. To avoid the leakage risk, further measurements should be carried out, which allows for the detection of the other risk zones. Finally, the dike crown should be rebuilt.

3.3. CCR Surveys

The capacitively-coupled resistivity method (also called the CCR method) is one of the fast-growing geophysical research techniques in the field of near-surface investigations [5,35,36].

The method allows us to determine the apparent resistivity of the ground by using cumbersome galvanic electrodes, which are pulled along the ground by a small vehicle or single person. The methods provide 2D or 3D field data for a few of depth levels [36,37]. The field data can be visualized as quality data (curves and pseudo-sections) or exported, and the inversion process can be applied.

The advantages of this method include the possibility to collect data quickly, in an almost continuous way. Secondly, (contrary to ERT) there is no requirement to put metal sticks into or on the ground. Finally, a high horizontal resolution results. One weakness of this method is it is only possible to apply the dipole-dipole array; therefore, collected data might experience inference [35,37].

In the studied area, the CCR method was applied using an OhmMapper TR1 capacitively-coupled resistivity meter [54]—www.geomatrix.co.uk, access date: 1 January 2022. The survey was carried out on the top of dike along P2 line (Figure 2A).

The CCR measurements were carried out in the continuous mode, where intervals were marked every 2 m. The OhmMapper geometry was set up using three receivers (Rx1–Rx3) and a standard single transmitter Tx. The applied settings are shown in Figure 11.

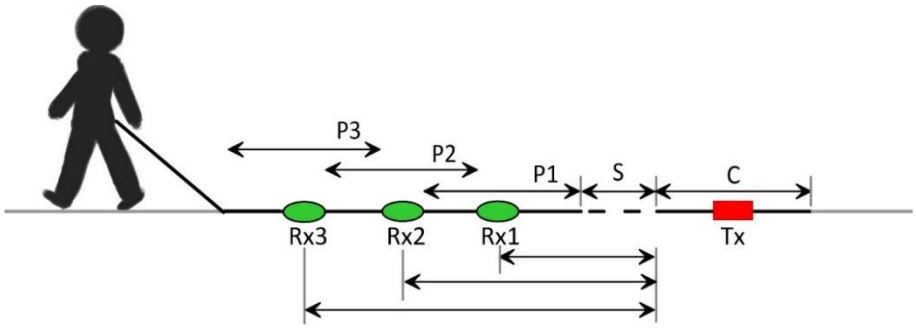

Figure 11. Schematic of the OhmMapper with three receivers (Rx) and a transmitter (Tx), being pulled by a single man; the potential dipoles (P1–P3), current dipole (C), and separation (S).

The detailed geometry of OhmMapper array was shown below, in Table 1.

Table 1. Geometry of the OhmMapper applied during the measurements.

Measuring Series	Rx3 [m]	Rx2 [m]	Rx1 [m]	S [m]	Tx [m]	Receivers Number
1	-	-	5	5	5	1
2	-	-	5	10	5	1
3	-	-	5	15	5	1
4	-	-	10	10	10	1
5	-	-	10	15	10	1
6	-	7.5	5	5	5	2
7	-	7.5	5	10	5	2
8	-	7.5	5	15	5	2
9	10	7.5	5	5	5	3
10	10	7.5	5	10	5	3

In the next stage, the obtained field data was analysed using OhmImager software version 1.1 (data analysis applet). In the software, the following steps were applied. Firstly, the data was examined. Then, the accuracy of the geometry was checked and, in some cases, adjusted. Secondly, the erroneous data was removed, in two ways, by deleting the individual pieces of data, as well as the use of a median filter. In that way, the prepared data was averaged in a horizontal direction because much of the data density occurred in this direction [54]. This process is called 'gridding', and it in this case that 5 m cell sizes were used, allowing for too dense meshes in the interpolation process to be avoided.

The processed data was inverted using the non-linear least squares method [55]. An apparent resistivity pseudo-section was applied as an initial model. To be precise, in the software, the 1D inversion process is realised, which means that the obtained data is treated as sounding curves. The inversion results are presented as a quasi-2D resistivity cross-section.

In order to compare the ERT and CCR data in Figure 10C (Section 3.2.), the 2D ERT and CCR resistivity cross-sections are shown.

In the CCR cross-section, the sand and gravel layers are visible. It is worth noting that its boundaries are far more blurred. In addition, the resistivity value, in the case of the high resistivity bodies, is a few times lower than of the ERT section. The low resistivity bodies have approximately the same resistivity value, as can be found in the ERT section. In addition, the sand and gravel layer, for distance x = 50–75 m and x = 22–30 m, are "stretched" to the zero (ground) level, which is not observed in the ERT section. This can probably be explained by the fact that the CCR data has a smaller data coverage in the vertical direction than that of the ERT method. Additionally, the size of the CCR dipoles is bigger than those used in the ERT method, which will influence the smaller resolution in the shallowest parts of ground. Therefore, the obtained data is approximated to the model limits.

To sum up, based on the CCR cross-section, there are no possible geological reasons as to why leakage zone no. I is present. Moreover, geological interpretation of the CCR data is restricted because of the wrong approximation of the resistivity values.

3.4. Seismic Surveys

Three seismic methods are useful for the study and inspection of dikes, they are: multichannel analysis of surface waves (MASW), seismic refraction (and, especially, its "automatic" version, known as seismic refraction tomography (SRT)), and high-resolution seismic reflection (HRSR).

The SRT and the HRSR are able to provide data about the contact dike body/substratum and mechanical impedances of dike structure. Reference [25] indicated the potential for MASW on dike inspection in a site in Germany, but poor results were obtained by the SRT. A complete review of MASW technique [56], used for dike inspection in the USA, is exhibited in the recent work of Moody [57], who concluded that MASW provides general information about dike structures, but its lateral resolution, which is capable of detecting local dike defects, is rather limited. Royet et al. [40] recommended the MASW and refraction techniques for dike inspection.

Generally, it seems that, for different countries, the guidelines established by evaluating several methods may differ; however, generally, the seismic methods are rarely used. As far as we know, there are no reports or recommendations for the use of the HRSR for dike inspection; meanwhile, this approach provides, theoretically, the best lateral resolution and, hence, the most efficient way to detect dike defects (between the above three methods).

This section presents the results of the HRSR, carried out along the profile indicated in Figure 12. As far as we know, this is the first use of the HRSR for such purposes in Poland. Similar to the studies presented in previous sections, the goal of this survey is to verify whether the HRSR approach is able to image the dike structure and locate the leakage zones. According to the general geological structure of inspected dike, it could be expected that the HRSR should detect two principal markers, shown in Figure 1. The first marker, noted at point 'A', is the interface between layers I and II and occurs at a depth

between 4–5 m (measured from the top of dike). The second marker, noted at point 'B', is the water table, located at a depth around 10 m from the top of the dike. It should, in principle, constitute an excellent seismic reflector, as its depth corresponds roughly to the Vistula water level and, therefore, will mask the interface between layers III and IV.

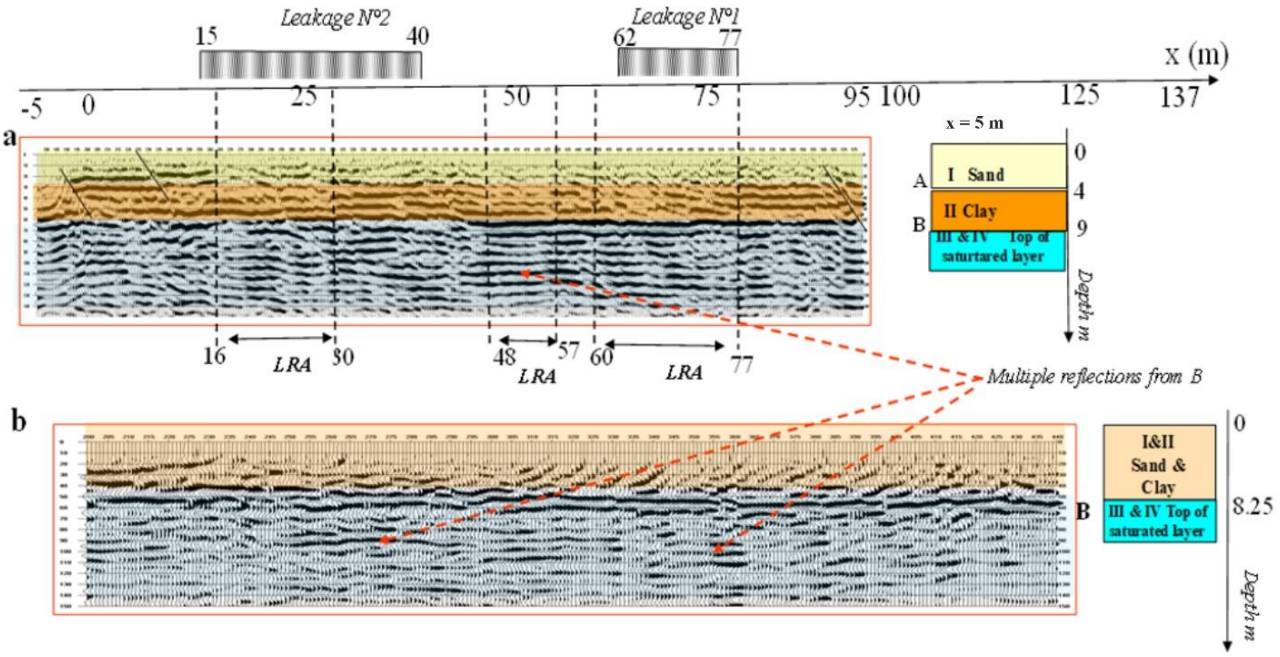

Figure 12. The high-resolution seismic reflection profiles obtained along the top of dike and their inter-pretation. (**a**) The 100 Hz profile, LRA symbols indicate the loss of reflection, straight black lines indicate shallow faults; (**b**) 26 Hz profile.

The difficulty of the HRSR method (in comparison with the "classic" deep seismic methodology) lies in the fact that the signals reflected from shallow targets are generally mixed with a background of coherent noise (CN), i.e., surface waves, ground roll, refractions, and air-coupled waves. Therefore, the principal way to discover the researched shallow reflections is to find the so-called optimum offset window (OOW) [33], that is, the offset interval where the reflection/CN ratio is most favourable, and to dispose of the data that has a sufficiently high frequency, in order to distinguish the shallow reflections from the background of CN [58].

It should be noted that the decrease of the depth of interest does not facilitate the work to be done, as could be expected. That is why progress in HRSR is measured by the decrease of the shallowest prospected depth [31,32,59]. In this context, the targeted depth of marker 'A' is close to 3–4 m, which is quite small, and such a case is referred to as a very high-resolution reflection seismic [60,61].

In terms of the pulse-echo imaging device, the seismic CDP gather is equivalent to sounding with the synthetic aperture array of dimension D (close to OOW length), focused (by using normal move out) at the subsurface point known as the CDP (common depth point) at depth d. The set of traces, presented as a function of CDP position, gives the final output image. The image's lateral resolution is assumed to be equal to the Fresnel radius ($\lambda_a d/2)0.5$), where λ_a is the apparent processed acoustic wavelength, $\lambda_a = V_{rms}/f_d$, V^{rms} is the stacking velocity, fd is the dominant signal frequency, and d indicates the depth. The depth resolution (Δr) within the first detected layer may be estimated to be $1/4\lambda_a$.

It should be noticed that, to achieve good depth and lateral resolutions, the use of short wavelengths is required, i.e., high frequencies. Since ground absorption increases with frequency, the highest exploitable frequency, f_d, is always limited and mostly depends on the source used. In the presented study, the optimal solution was to use the wide-

banded explosive type Betsy [62–64], but the use of such a source was prohibited because of its destructive nature. Finally, the sledgehammer (one blow, no stacking) was used as the source.

Two HRSR profiles were carried out along the line indicated in Figure 1 using a 48-channel Geometrics Strata Visor NZXP seismograph manufactured in the USA, San Jose. End-off geometry was applied (in order to get a better velocity estimation), and the closest offset was kept constant (source and receivers were rolled by the receiver spacing), in order to keep the OOW constant.

3.4.1. The 100 Hz Profile

The goal of the first profile referred as the "100 Hz profile" was to detect the I/II interface (marker 'A'), and its geometry was set, in order to obtain as high a resolution as possible. Acquisition was carried out using 100 Hz geophones, which provided the primary low-cut filtering of the seismic data [58]. The nearest offset, chosen with the respect to depths of marker 'A', was set to 1 m. According to principles used for research of anomalies [57], the geophone spacing was set to 0.5 m, yielding a CDP resolution of 0.25 m. The profile was processed using Winses18 software, version 1.8 [65] and applying the HRSR CDP processing flow, that is: input band pass filtering, first arrival and air-coupled wave muting, FK filtering, scaling, optimum offset window (OOW) applied (offset windowing), velocity analysis, NMO correction, CDP stacking, and post-stack band pass filtering. The OOW for this profile fits the offset interval between 3–8 m for marker 'A' and 7–20 m for marker 'B'. The geometry and essential parameters of this profile are summarized in Table 2.

Table 2. Geometry and basic resolutions of two HRS profiles.

Profile Name	Geophones Used	Source	Number of Shots	Profile Limits xmin/xmax (m)	Minimum Source Receive Offset (m)	Geophone Spacing (m)	CDP Spacing (m)	Dominating Frequency in Stacked Section	Dominating Wavelength in the First Layer (m)	Depth Resolution in the First Layer (m)	Lateral Resolution at m Depth of Marker A
100 Hz	100 Hz	Sledgehammer 5 kg	194	0/100	1	0.5	0.25	100	3	0.75	2.1
26 Hz	26 Hz	Sledgehammer 5 kg	139	0/125	6	1	0.5	120			

The obtained seismic section and its interpretation are shown in Figure 12a. It can be seen that the profile displays the "natural" geological structure, indicated in Figure 1, and reveals the expected markers 'A' and 'B'. The depth of marker 'A' is close to 4 m and correlates with the depths obtained by bore holing and GDR (Figures 8 and 9). The depth of marker 'B', close to 9 m, is a little greater than the water table detected by bore holing (Figure 1, 6–7 m)). The obtained interval velocities for layers I and II are shown in Table 3. These velocities were independently checked by refraction and provide similar results. The obtained values agree with the velocities occurring in dikes, as reported by Moody [51].

Table 3. Velocities in detected layers I and II, obtained from the HRSR 100 Hz profile and refraction (one arbitrarily chosen shot of the profile beginning).

		Obtained from HRSR x = 5 m		Obtained from Refraction	
Layer	**Material**	**Depth (m)**	**Interval P Velocity (m/s)**	**Depth (m)**	**Velocity (m/s)**
I	sand	4	282	3.0–3.5	280
II	clay	6	520	8.2–9.0	550
III	Saturated ground	-	-	-	1500–1550

Notice that marker 'A' is not continuous. Three zones 16–3, 48–57, and 60–77 m are characterised by a significant weakening and even disappearing of marker 'A'. They are indicated in the figure as the intervals 'Loss of Reflection from A' (LRA). The first and third zones correlate reasonably well with the leakage zones; therefore, they might be interpreted as the induced perturbations of the deteriorated part of the interface between the sand and

clay. Remaining zones 0–16, 30–48, 57–60, and 77–95 m show marker 'A' correctly, and this suggests that the dike is stable there. Furthermore, the deteriorated part of interface between the sand and clay may be larger than the observed leakage limits; therefore, the second zone, 48–57 m (which does not correlate with the leakage zones), may also indicate the deteriorated part of this interface.

Independently three symptoms of shallow faults are observed, at positions, 7, and 92 m. It is difficult to explain their nature, but they may indicate the weaker points of the dike, with the risk of leakage during an eventual future flood.

Concerning the reflection from the water table, the marker 'B' is strong and continuous (as expected). No anomalies linked with leakage zones are observed, thus indicating that dike destruction occurs mainly in layer I at the depth of marker 'A'. The reflection from 'B' is so strong that the multiple reflections between 'B' and the ground surface occur (indicated in the Figure 12).

3.4.2. The 26 Hz Profile

The goal of the second profile was to provide an image of a deeper geological structure exceeding the water table depth. Therefore, the signal frequency was lowered by using 26 Hz geophones. The acquisition parameters are summarized in Table 3. Processing the lower bandwidth, 40–90 Hz, showed that the deeper structure is strongly masked by multiple reflections between the water table and the surface. Therefore, the processing was oriented towards the high-resolution imaging of marker 'B'. The obtained image is shown in Figure 12b. Since the 26 Hz geophones are more sensitive than the 100 Hz model, and the seismograph gain was set to high, the archived dominating frequency in the stacked section is even higher than that of the 100 Hz section (see Table 2), thus enabling further image details of marker 'B'. Indeed, marker 'B' displayed more small perturbations than was seen in the Figure 12a) (due to the higher resolution); however, they cannot be interpreted as the anomalies within the dike.

This work is significant in that it demonstrates that a single sledgehammer blow, along with the use of 26 geophones, is sufficient to reach the water table. An even better resolution Hz can be achieved when using 100 Hz geophones. This shows that, in the future, a setup including a sledgehammer and streamer, composed of 26 Hz geophones with geometry used for a 100 Hz profile Hz towed along the dike crown, can be more than adequate for obtaining images of both markers 'A' and 'B'. Note that the same acquisition setup can also independently provide the seismic data for the MASW and SRT methods.

4. Global Interpretation

4.1. Geological Model of Inspect Dike

All of the applied geophysical techniques are characterized by a different depth of investigation, vertical and horizontal resolution, and sensitivity for other physical parameters. Hence, a comprehensive approach to the contextual interpretation should permit more reliable geological models of the studied dike.

Based on the ERT survey, the deepest part of the studied area is the water table. The layer top is about 6 to 8 m below the ground surface on the landside and directly beneath the crown dike. The above interpretation is also confirmed by the seismic results, where the mentioned border is interpreted as 9 m below the ground surface. The GPR depth of the investigation is too low in this case, which is caused by the presence of the good conducted medium. It is worth noting that the water label for the second profile line (dike crown) is characterized by the resistivity value higher than other cases/profiles. The mentioned fact is bonded with a specific geometry of the levee, which changes the electrical field distribution, while the main assumption of the inversion process is the presence of the 2D geometry of the studied medium.

Another geological layer consists of fluvio-glacial and fluvial sand and gravel, which are clearly visible in the ERT. Based on the interpreted resistivity from the ERT method, which is about 2500 Ωm, it can be assumed that the sands and gravels are poorly sorted [31].

The mentioned sediments are characterized by an extremely high water permeability. The top of the sand and gravel mixture is from 2 (the landside) to 5 m (the waterside) below the ground level. In the case of the P2 profile, the sands and gravel are directly beneath the dike crown. Moreover, the dike part, from 27–40 and 50–75, was built up with this kind of material, which explains why the leakage zones occurred. In addition, the GPR results suggest that the dike crown from 30–80 m is built from unconsolidated and weathered material. In the ERT method, this change in the dike structure is difficult to identify.

Outside the crown dike, the sand and gravel are covered by clays, partly mixed with sands/gravel, which can be attributed to the raised resistivity value. On the landside, the average thickness of the layer is about 2 m. The layer is unconsolidated and weathered, which aligns with the GPR results. On the other side of the dike, the thickness is about two times bigger, which is the effect of accumulative action of the river. This fact is confirmed by a reduction of amplitudes in the echograms.

In the matter of the geological and geophysical data correlation, in the geological boreholes visible, is a relatively thin layer of clay. None of the applied methods were able to detect this layer because there was not enough vertical resolution.

4.2. Zones of Leakage Risk (Hazard Zones)

A summary of the results, concerning the research of the hazard zones, is presented in Table 4. The hazard zones, detected by GDR as the abnormal increase from marker 'A', occur between 22–40 and from 50–75 m of the profile length. At the same time, the hazard zones, detected by HRSR as the decrease or total loss of reflection from marker 'A', occur at intervals 16–30, 48–57, and 60–77 m.

Table 4. Summary of used methods and of the detected hazard zones.

Method	Reference Figure	Interpreted Symptoms	Examined Dike Zone x(m)	Detected Hazard Zones x(m)
GPR 200 MHz Polarization co-pole	Figure 6	Method does not provide any information about hazard zones	0–200	-
GPR 200 MHz Mixed polarisation	Figure 8b,c Figure 9	Abnormal stronger reflection level from reflector 'A'	0–150	25–65 135–145
ERT	Figure 10b	High resistivity anomalies—sands with the extremely high-water permeability	0–75	22–40, 50–75
CCR	Figure 13	Method does not provide any information about hazard zones	0–75	-
HRS 100 Hz	Figure 12a	Unusual decrease or total loss of reflection from marker 'A'	5–98	16–30 48–57 60–77

Notice that GDR detects the anomalies of marker 'A' as the zone of increased reflections from 'A'; meanwhile, HRSR inversely shows the unusual total loss of reflection from marker 'A'. This could be explained by the fact that the em "sees" the higher ground resistivity, corresponding to dried canals created by water during the leakage. At the same time, the seismic wave seems to be distorted by the irregularities of interface 'A', caused by its damage. Instead of being reflected, the wave is diffused, CDP signals gathered are badly correlated, and final stacked signal weakens or disappears. Similar effects are observed during the detection of underground voids.

In turn, initial dike recognition using the ERT method allowed for the interpretation of the high resistivity (dry) sand and gravel as risk zones. The mentioned sediments are directly below the bottom of the dike and partly consists of its building material.

The sediments are characterized by an extremely high value of permeability. Thereupon, during flooding, water can easily travel to the body of the dike and flow outside the dike construction (landside).

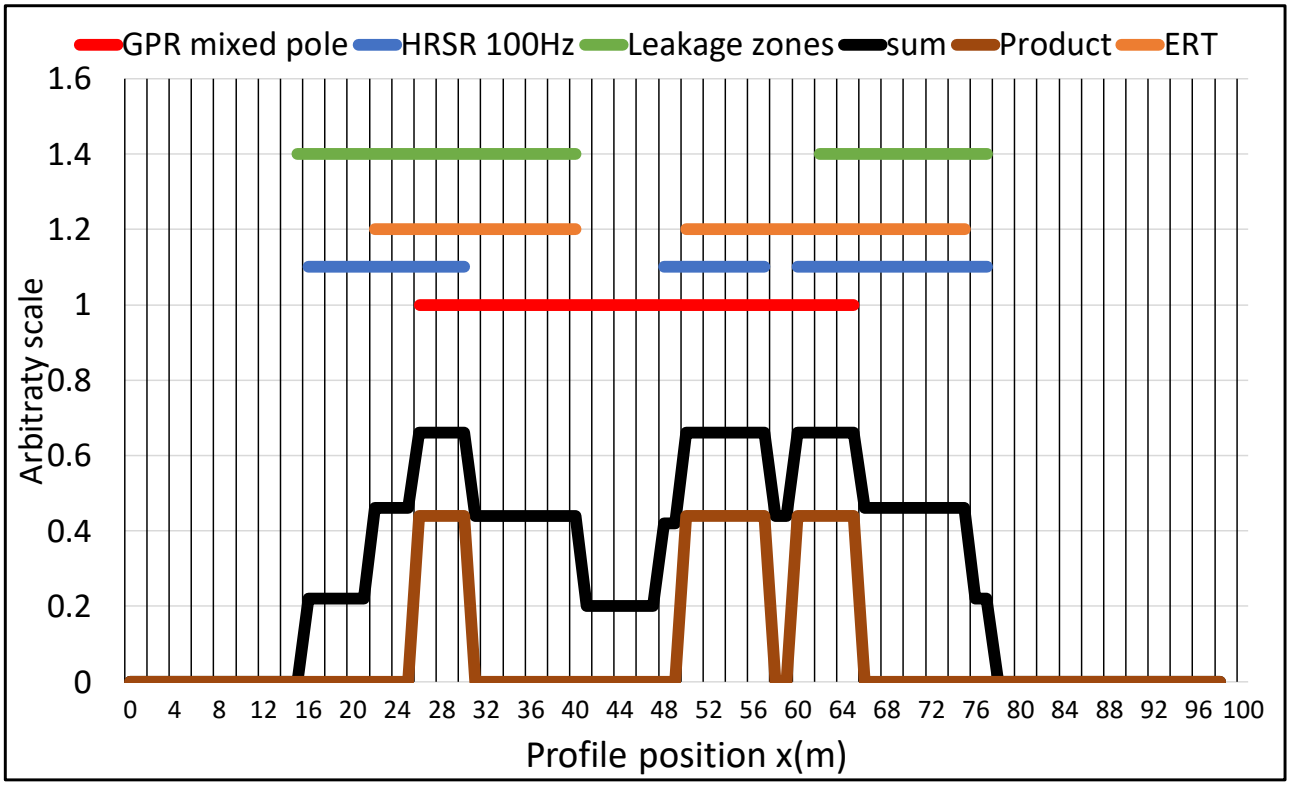

Figure 13. Symbolic illustration of detected hazard zones, detected by GPR, ERT, and HRSR, in profile intervals between 0 and 100 m. The "sum" and "product" denote, respectively, the scales fusion of three used methods by using the fussy logic: the logic "or" and logic "and", respectively.

The other methods (GPR co-pole and CCR) do not provide conclusive proof of any hazard presence.

The detected hazard zones, by the GPR, ERT, and HRS, are also symbolically illustrated in Figure 13, which enables a visual comparison of the location of detected anomalies within leakages I and II.

In order to combine the GPR, ERT, and HRSR results, a simplified fusion of the obtained results, using the scaled logic sum and scaled product of the hazard d areas (coded in binary scale as 1 or 0), was performed using the simplified fuzzy logic technique (used in multi-approach surveys) [66]. The sum (logic or) correlates positively with the leakage area. It should be noted that the leakage limits do not necessarily correspond with the zone of the destruction of the sand/clay interface, and this may be a larger risk. Visually, the HRSR and ERT results provide the best correlation with the leakage zones. At the same time, the logic product (logic and) can be interpreted as the most probable hazard zones.

5. Conclusions

The geological model of the inspected dike was realised by constructing geophysical models, which were then correlated with the data about spotted leakages zones.

The geological interpretation of the geophysical cross-sections was supported with data from the shallow geological boreholes and geotechnical probes. The common interpretation enabled the detection of geophysical anomalies, which correlated with the leakages spots. The applied methodology enabled the isolation of areas that could be dangerous during the next floods.

The interpretation of the conducted geophysical, geotechnical, and laboratory measurements suggest that there is a risk of leakage zones appearing or, equally, some parts of the dike will be destroyed. From a geological point of view, the studied area is dominated by the clays that create the Vistula riverbed. The shallowest layer is the water table

sand/gravel. The presence of sand and gravel between the mentioned layers is problematic because of their high-water permeability. Moreover, the sediments are located directly beneath the dike crown and consist of its building material.

The ERT method allowed for the recognition of general geological settings, which correlated with the leakage zones with the resistivity anomalies. The GPR method allowed us to create a more detailed picture of the subsurface zone. The HRSR shows the expected geological structure, i.e., layers I and II, and accurately map their depth. The CCR method shows a more general picture, and the high resistivity anomalies are poorly mapped.

Concerning the detection of hazard zones, it is shown that the combined use of mixed pole GPR, ERT, and HRSR methods may be useful for the detection of the anomalies on the sand/clay interface, which seem to be related to old or future leakage zones. The GPR method roughly indicates the zone of risk. The ERT method, supported by the petrophysics lab test results, may explain why, in some places, leakage zones appear. The HRSR method shows the locations of the anomalies, with a relatively high accuracy. Therefore, and since the HRSR method is known to be cost effective, it is recommended for use along the previously selected zones, identified using the GPR method, as a low cost and rapid method. Furthermore, according to the conclusions in Section 3.4, it seems that the cost effectiveness of the HRSR method can be improved by using a setup comprising of a sledgehammer and towing a 26 Hz geophone streamer. The same setup can independently provide the seismic data for the MASW method (not treated in this paper), largely used for dike evaluation and the SRT method.

The proposed methodology was tested in the early chosen area, where the leakage was spotted. For example, based on the resistivity distribution in the studied levee, it can be said the leakage areas are the relatively high resistivity anomaly (sand and gravel) against relatively low resistivity medium/sandy clay. Based on the interpreted resistivity cross-section in the Figure 10, it is also a possible case where the levee body will be built with the use of sandy material. That will cause there to be no condition of applying the geophysical methods met, where contrast of the physical parameters is required. The mentioned problem refers to all geophysical methods. It seems the main limitation of the proposed methodology.

In general, the main difference between the performed study and literature is connected with the CCR method. In the available literature, the CCR results are closer to the ERT results and, in some cases, even practically identical. In our study, the mentioned results show a very generalized form of the ERT cross-section. The reason for this is probably the spacing between the transmitter and receivers being too high, as well as there not being enough data levels. Another reason may be connected with an applied inversion software. In the literature, the most commonly applied software is Res2dinv [42]; in the case shown, the OhmMapper manufactured software was used [54]. In the next step, the obtained CCR data will be reinterpreted with the Res2Dinv software. In the case when this operation does not get better quality inverted data, the CCR methodology will be changed.

Author Contributions: Conceptualization, T.G., B.P. and M.Ć.; methodology, T.G., B.P. and M.Ć.; software, T.G., B.P. and M.Ć.; validation, T.G., M.Ć. and B.P.; formal analysis, T.G., B.P. and M.Ć.; investigation, T.G., B.P. and M.Ć.; resources, T.G., B.P. and M.Ć.; data curation, T.G., B.P. and M.Ć.; writing—original draft preparation, T.G., M.Ć. and B.P.; writing—review and editing, T.G., M.Ć. and B.P.; visualization, T.G., M.Ć. and B.P.; supervision, T.G., B.P. and M.Ć.; project administration, T.G., M.Ć. and B.P.; funding acquisition, T.G., M.Ć. and B.P. All authors have read and agreed to the published version of the manuscript.

Funding: This research was funded by the grant EMMA (i.e., E-Mobility, Sustainable Materials and Technologies), no. PPI/APM/2018/1/00027/U/001—task no. 9, within cooperation between the Cracow University of Technology (Poland) and Ecole Centrale de Lille (France). The project was supported by the Polish National Agency for Academic Exchange research program. The works were also supported by the "Poli Doctus" scholarship, as part of the project: POWER—"A Way to Perfection—a comprehensive university support program".

Institutional Review Board Statement: Not applicable.

Informed Consent Statement: Not applicable.

Data Availability Statement: The data is available in the disk archive at the Department of Geoengineering and Water Management at the Faculty of Environmental and Power Engineering at the Krakow University of Technology and is not available outside.

Acknowledgments: The work presented in this paper was performed in the framework of the grant EMMA (i.e., E-Mobility, sustainable Materials and Technologies), no. PPI/APM/2018/1/00027/U/001—task no. 9, within cooperation between the Cracow University of Technology (Poland) and Ecole Centrale de Lille (France). The project was supported by the Polish National Agency for Academic Exchange research program. We also appreciate the "Poli Doctus" scholarship, as part of the project: POWER—"A Way to Perfection—a comprehensive university support program".

Conflicts of Interest: The authors declare no conflict of interest.

References

1. Gąsiorowski, S. *Budowa Ziemnych Wałów Przeciwpowodziowych, a Stablizacja Gruntu*; Technika; Kwartalnik kosztorysanta: Warszawa, Poland, 2012.
2. Gołębiowski, T. Velocity Analysis in the GPR Method for Loose Zones Detection in the River Embankments. In Proceedings of the International GPR Conference, Lecce, Italy, 21–25 June 2010.
3. Gołębiowski, T. Changeable-offset GPR Profiling for Loose Zones Detection in the Levees. In Proceedings of the Near Surface Conference, Cracow, Poland, 15–17 September 2008.
4. Gołębiowski, T. *Application of the GPR Method for Detection and Monitoring of Objects with Sochastical Distribution in the Geological Medium*; AGH-UST: Kraków, Poland, 2012.
5. Gołębiowski, T.; Małysa, T. The Application of GPR Method for Detection of Loose Zones in Flood Levee. In Proceedings of the E3S Web of Conferences, Cracow, Poland, 7–8 June 2018; Volume 30.
6. Gołębiowski, T.; Małysa, T. The Application of Non-standard GPR Techniques for the Examination of River Dikes. *Czas. Tech.* **2018**, *7*, 121–138.
7. Gołębiowski, T.; Ostrowski, T. Application of Geoelectrical Techniques form Examination of Subsoil of Hydrotechnical Constructions. In Proceedings of the Scientific and Technical Conference on Application of Computer Methods for Designing and Analysis of Hydrotechnical Constructions, Korbielów, Poland, 27 February–1 March 2017.
8. Gołębiowski, T.; Pasierb, B.C.R. Complex Detection of Loose Zone in Flood Dikes. In Proceedings of the Scientific and Technical Conference on Application of Computer Methods for Designing and Analysis of Hydrotechnical Constructions, Korbielów, Poland, 2015.
9. Gołębiowski, T.; Piwakowski, B.; Ćwiklik, M. Application of the GPR and ERT Methods for Non-invasive Examination of Flood Dike. In Proceedings of the Scientific and Technical Conference MATBUD, Cracow, Poland, 19–24 October 2020.
10. Gołębiowski, T.; Tomecka-Suchoń, S.; Farbisz, J. Application of Complex Geophysical Metods for Non-invasive Examination of Technical Conditions of Flood Dikes. In Proceedings of the European Symposium on Anti-flood Defences, Paris/Orleans, France, 28–30 March 2012.
11. Guy, E.; Daniels, J.J.; Radzevicius, S.; Vendl, M. Demonstration of Using Crossed Dipole GPR Antenna for Site Characterization. *Geophys. Res. Lett.* **1999**, *26*, 3421–3424. [CrossRef]
12. Marcak, H.; Gołębiowski, T. The Use of GPR Attributes to Map a Weak Zone in a River Dike. *Explor. Geophys.* **2014**, *45*, 123–133. [CrossRef]
13. Marcak, H.; Gołębiowski, T.; Tomecka-Suchoń, S. Analysis of Possibility of Using the GPR Refraction for Location Changes in River Embankments. *Geology* **2005**, *31*, 3–4.
14. Cygal, A.; Borecka, A.; Stefaniuk, M.; Sada, M.; Ważny, J. Multivariate interpretation geophysical data for evaluation of geotechnical condition of part embankment Vistula river. In Proceedings of the CAGG AGH Conference, Kraków, Poland, 10–13 September 2019.
15. Cygal, A.; Stefaniuk, M.; Kret, E.; Klityński, W. Zastosowanie metody konduktometrycznej do typowania stref o zmiennych parametrach filtracyjnych w obrębie podstawy wału przeciwpowodziowego. *Przegląd Geol.* **2015**, *63*, 652–656. (In Polish)
16. Cygal, A.; Stefaniuk, M.; Kret, E.; Kurowska, M. The application of electrical resistivity tomography (ERT), induced polarization (IP) and electromagnetic conductivity (EMC) methods for the evaluation of technical condition of flood embankment corpus. *Geol. Geophys. Environ.* **2016**, *42*, 279–287. [CrossRef]
17. Dahlin, T.; Löfroth, H.; Schälin, D.; Suer, P. Mapping of quick clay using geoelectrical imaging and CPTU-resistivity. *Near Surf. Geophys.* **2013**, *11*, 659–670. [CrossRef]
18. Dahlin, T.; Zhou, B.A. Numerical Comparison of 2D Resistivity Imaging with Ten Electrode Arrays. *Geophys. Prospect.* **2004**, *52*, 379–398. [CrossRef]
19. Dunbar, J.B.; Smullen, S.; Stefanov, J.E. The Use of Geophysics in Levee Assessment. In *Symposium on the Application of Geophysics to Engineering and Environmental*; Environmental & Engineering Geophysical Society: Denver, CO, USA, 2007.

20. Hayashi, K.; Abe, T.; Tanaka, T.; Konishi, C. Application of integrated geophysical method to levee evaluation. In Proceedings of the Fourth International Conference on Scour and Erosion, Tokyo, Japan, 5–7 November 2008; pp. 295–301.
21. Hayashi, K.; Konishi, C. Joint Use of a Surface-Wave Method and a Resistivity Method for Safety Assessment of Levee Systems. In Proceedings of the GeoFlorida 2010: Advances in Analysis, Modeling & Design, Orlando, FL, USA, 20–24 February 2010.
22. Oh, S. Safety Consideration of Embankment by Conditional Analysis of Electrical Resistivity. In Proceedings of the Near Surface 2008, 14th European Meeting of Environmental and Engineering Geophysics, Kraków, Poland, 15–17 September 2008.
23. Sjödahl, P.; Dahlin, T.; Johansson, S. Using the resistivity method for leakage detection in a blind test at the Røssvatn embankment dam test facility in Norway. *Bull. Eng. Geol. Environ.* **2010**, *69*, 643–658. [CrossRef]
24. Oryński, S.Z.; Foltyn, N. Flooded zones recognition with the use of Ground Conductivity Meters. In Proceedings of the 77th EAGE Conference & Exhibition, Madrid, Spain, 1–4 June 2015.
25. Niederleithinger, E.; Weller, A.; Lewis, R. Evaluation of Geophysical Techniques for Dike Inspection. *J. Environ. Eng. Geophys.* **2012**, *17*, 185–195. [CrossRef]
26. Lundström, K.; Larsson, R.; Dahlin, T. Mapping of quick clay formations using geotechnical and geophysical methods. *Landslides* **2009**, *6*, 1–15. [CrossRef]
27. Karl, L.; Fechner, T.; Schevenels, M.; François, S.; Degrande, G. Geotechnical characterization of a river dyke by surface waves. *Near Surf. Geophys.* **2011**, *9*, 515–527. [CrossRef]
28. Cichostępski, K.; Dec, J.; Kwietniak, A. Relative amplitude preservation in high-resolution shallow reflection seismic: A case study from Fore-Sudetic Monocline, Poland. *Acta Geophys.* **2019**, *67*, 77–94. [CrossRef]
29. Cichostępski, K.; Dec, J.; Kwietniak, A. Simultaneous Inversion of Shallow Seismic Data for Imaging of Sulfurized Carbonates. *Minerals* **2019**, *9*, 203. [CrossRef]
30. Cichostępski, K.; Dec, J. Estimation of Shallow Sulphur Deposit Resources Based on Reflection Seismic Studies and Well Logging. *Energies* **2021**, *14*, 5323. [CrossRef]
31. Branham, K.L.; Steeples, D.W. Cavity detection using high-resolution seismic reflection methods. *Min. Eng.* **1988**, *40*, 115–119.
32. Brouwer, J.; Helbig, K. *Shallow High-Resolution Reflection Seismics*; Elsevier: Amsterdam, The Netherlands, 1998.
33. Cook, J.C. Seismic mapping of underground cavities using reflection amplitude. *Geophysics* **1965**, *30*, 527–538. [CrossRef]
34. Łój, M.; Porzucek, S.; Gołębiowski, T.; Everett, M.E. Microgravimetric and GPR Surveys for Detection of Unconsolidated Zones in a Levee. In Proceedings of the E3S Web of Conferences, Cracow, Poland, 7–8 June 2018; Volume 66.
35. Ball, L.B. *Capacitively Coupled Average Resistivity of the Interstate and Tri-State Canals*; Scientific Investigations Report; U.S. Geological Survey Lincoln: Lincoln, NE, USA, 2006.
36. Garman, K.M.; Purcell, S.F. Applications for capacitively coupled resistivity surveys in Florida. In Proceedings of the 17th EEGS Symposium on the Application of Geophysics to Engineering and Environmental Problems, Colorado Springs, CO, USA, 22–26 February 2004; Volume 23, pp. 697–698.
37. Kuras, O.; Beamish, D.; Meldrum, P.I.; Ogilvy, R.D. Fundamentals of the capacitive resistivity technique. *Geophysics* **2006**, *71*, G135–G152. [CrossRef]
38. Timofeev, V.M.; Rogozinski, A.W.; Hunter, J.A.; Douma, M. A new ground resistivity method for engineering and environmental geophysics. In *Symposium on the Application of Geophysics to Engineering and Environmental Problems 1994*; Environmental & Engineering Geophysical Society: Denver, CO, USA, 1994; pp. 701–715.
39. Fauchard, C.; Mériaux, P. *Geophysical and Geotechnical Methods for Diagnosing of Flood Protection Dikes*; éditions Quae: Versailles, France, 2007.
40. Royet, R.; Palma-Lopes, S.; Fauchard, C.; Mériaux, P.; Auriau, L. *Reliability of Urban Flood Defences—Rapid and Cost-Effective Dike Condition Assessment Methods: Geophysics and Remote Rensing*; FloodProBE—Project report of grant agreement no: 243401; FloodProBE: Orleans, France, 2013.
41. Kot, A. *Expertise of Technical Condition of Flood Gate No. 1 Located in the Left Flood Dike of the Vistula River in the Village of Wawrzeńczyce*; Aquin firm Ed.: Auschwitz, Poland, 2013.
42. Annan, A.P. *Ground Penetrating Radar*; Sensor & Software: Mississauga, ON, Canada, 2005.
43. ReflexW. *User Guide*; Sandmeier Geophysical Research: Karlsruhe, Germany, 2019.
44. Robert, R.L.; Daniels, J.J. Analysis of GPR polarization phenomena. *J. Environ. Eng. Geophys.* **1996**, *1*, 139–157. [CrossRef]
45. Szalai, S. About The Depth of Investigation of Different D.C. Dipole-Dipole Arrays. *Acta Geod. Geophys. Hung.* **2000**, *35*, 63–73.
46. Szalai, S.; Szarka, L. An approximate analytical approach to compute geoelectric dipole-dipole responses due to a small buried cube. *Geophys. Prospect.* **2000**, *48*, 871–885. [CrossRef]
47. Loke, M.H. 2-D and 3-D Electrical Imaging Surveys. Tutorial Geotomo Software, 2003. Available online: www.geotomosoft.com/downloads.php (accessed on 1 January 2022).
48. Loke, M.H. Rapid 2D Resistivity & IP Inversion Using Least-Squares Method. Tutorial Geotomo Software, 2010. Available online: www.geotomosoft.com/downloads.php. (accessed on 1 January 2022).
49. Loke, M.H.; Ackworth, I.; Dahlin, T. A comparison of smooth and blocky inversion methods in 2D electrical imaging surveys. *Explor. Geophys.* **2003**, *34*, 182–187. [CrossRef]
50. Papadopoulos, N.G.; Tsourlos, P.; Tsokas, G.N.; Sarris, A. Two-dimensional and three-dimensional resistivity imaging in archaeological site investigation. *Archaeol. Prospect.* **2006**, *13*, 163–181. [CrossRef]
51. Aspinall, A.; Saunders, M.K. Experiments with the square array. *Archaeol. Prospect.* **2005**, *12*, 115–129. [CrossRef]

52. Keller, G.V. Electrical properties of rocks and minerals. In *Handbook of Physical Constants*; CRC Press: Boca Raton, FL, USA, 1966; pp. 283–292.
53. Kobranova, V.N. *Petrophysics*; Springer: Berlin/Heidelberg, Germany, 1989.
54. OhmImager Manual. *OhmImager Software for Data Analysis of the OhmMapper*; Version 1.1; GEOMATRICS: San Jose, CA, USA, 2014.
55. Ghosh, D.P. The application of linear filter theory to the direct interpretation of geoelectrical resistivity sounding measurements. *Geophys. Prospect.* **1971**, *19*, 192–217. [CrossRef]
56. Foti, S.; Lai, C.G.; Glenn, J.; Strobbia, C. *Surface Wave Methods for Near-Surface Site Characterization*; CRC Press: Boca Raton, FL, USA, 2015.
57. Moody, T.A. Geophysical Assessment of Kinion Lake Dam. Graduate Thesis, University of Arkansas, Fayetteville, AR, USA, 2017; p. 2470. Available online: http://scholarworks.uark.edu/etd/2470 (accessed on 1 December 2021).
58. Knapp, R.W.; Steeples, D.W. High resolution common-depth-point seismic reflection profilling: Field acquisition parameter design. *Geophysics* **1986**, *51*, 283–294. [CrossRef]
59. Kourkafas, P.; Goulty, N.R. Seismic reflection imaging of gypsum mine working at Sherburn-in-Elmet. *Eur. J. Environ. Eng. Geophys.* **1996**, *1*, 53–63.
60. Ghose, R.; Nijhof, V.; Brouwer, J.; Matsubara, Y.; Kaida, Y.; Takahashi, T. Shallow to very shallow high-resolution reflection seismic using a portable vibrator system. *Geophysics* **1998**, *63*, 1295–1309. [CrossRef]
61. Piwakowski, B. From high resolution land seismic imaging to very high resolution: State of the art, limits and field examples. Invited paper special HRS session. In Proceedings of the International Symposium of European Association of Exploration Geophysicists, Paris, French, 6–10 June 2004.
62. Doll, W.E.; Miller, R.D.; Xia, J. A non-invasive shallow seismic source comparison on the Oak Ridge Reservation, Tennessee. *Geophysics* **1998**, *63*, 1318–1331. [CrossRef]
63. Kosecki, A.; Piwakowski, B.; Driad-Lebeau, L.; Safinowski, P. *High Resolution Seismic Investigation in Salt Mining Context Part I: Comparison of Seismic Sources*; EAEG: Helsinki, Finland, 2006.
64. Miller, R.D.; Pullan, S.E.; Waldner, J.S.; Haeni, F.P. Field comparison of seismic sources. *Geophysics* **1986**, *51*, 2067–2092. [CrossRef]
65. Available online: www.kgs.ku.edu/software/winseis/index.html (accessed on 1 January 2022).
66. Leblanc, G.; Lee, M.; Morris, W. A simple adaptable data fusion methodology for geophysical exploration. *Explor. Geophys.* **2012**, *43*, 190–197. [CrossRef]